Available online at www.sciencedirect.com
SCIENCE DIRECT®
Journal of Organometallic Chemistry 689 (2004) 3242–3250
Journal of Organometallic Chemistry
www.elsevier.com/locate/jorganchem

Non-covalent assemblies of negatively charged boronated porphyrins with different cationic moieties

Afaf R. Genady [a,*], Mohamed E. El-Zaria [a], Detlef Gabel [b]

[a] Department of Chemistry, Faculty of Science, University of Tanta, 31527 Tanta, Egypt
[b] Department of Chemistry, University of Bremen, P.O. Box 330440, D-28334 Bremen, Germany

Received 20 April 2004; accepted 13 July 2004
Available online 20 August 2004

Abstract

A unique approach to non-covalent electron and energy transfer is described that is based on the formation of salt bridges between oppositely charged porphyrin units. A new class of electrostatically linked dimeric and pentameric porphyrins was synthesized by interaction of novel anionic boron containing porphyrins such as 5-(benzamidodecahydro-*closo*-dodecaborate)-10,15,20-triphenylporphyrin (N1) and *meso*-*tetrakis*-benzamidodecahydro-*closo*-dodecaborate)porphyrin (N2) and a variety of cationic *meso*-tetraarylporphyrin units. A bipyridine linked dimer (N1 · bpy · N1) was also prepared by employing *N*,*N*′-dimethyl-4,4′-bipyridinium (bpy) as a spacer between two mono-anionic species. A quinone-porphyrin dyad was also prepared for electron or energy transfer demonstration. All the synthesized assemblies were characterized by NMR, IR, UV–Vis, and mass spectroscopy. Significant spectral changes occurred in the absorption spectra of these non-covalent porphyrin assemblies compared to those of the reference monomers, indicating the presence of electronic interaction between the adjacent porphyrin units. Resonance light scattering was also used to study the formation of these assemblies in solution.

Keywords: Ionic porphyrin; Borane; Porphyrin assemblies; Optical spectra; Resonance light scattering

1. Introduction

Weak, non-covalent forces play key roles in the faithful replication of DNA, the folding of proteins into intricate three-dimensional forms, the specific recognition of substrates by enzymes, and the detection of single molecules. Indeed, all biological structures and processes depend on the interplay of non-covalent as well as covalent interactions. Charged porphyrins have attracted considerable attention since their first reported syntheses almost three decades ago [1,2] chiefly because of their remarkable ability to form complexes with and cleave nucleic acids [3]. Since the molecular recognition of DNA is of fundamental importance to life, analyzing the interaction of small molecules with DNA continues to be an important area of research. Within the context of this general theme, evidence that closely coupled porphyrin-related structured are involved in bacterial or plant photosynthesis has led to much recent work on such associated systems in vitro, in which a number of covalently linked porphyrin "dimers" or higher complexes have been synthesized by various means. Considerable debate within the electron transfer/photosynthetic modeling community continues, to be devoted to the question how specific protein pathways might, or might not, be concerned with salt bridges, and this, in turn, has focused renewed attention on electrostatically linked, non covalently assembled, and donor–acceptor conjugates [4,5]. Unfortunately, the available porphyrin assemblies, which could serve as simple salt-bridge-containing energy or electron transfer model systems, are all

* Corresponding author. Tel.: +2 40 3297974; fax: +2 40 3350804.
E-mail address: afafgenady@hotmail.com (A.R. Genady).

0022-328X/$ - see front matter © 2004 Elsevier B.V. All rights reserved.
doi:10.1016/j.jorganchem.2004.07.029

characterized by a face-to-face orientation between the relevant redox active partners [6,7]. Thus, there is a clear need at present for electrostatically assembled donor–acceptor systems that enforce alternative geometries. We here report the preparation and some properties of dimeric and aggregated structures formed simply by spontaneous association of cationic and anionic porphyrins.

Anionic porphyrins 5-(benzamidodecahydro-*closo*-dodecaborate)-10,15,20-*tris*- phenylporphyrin (N1) and *meso*-*tetrakis*-(benzamidodecahydro-*closo*-dodecaborate)porphyrin (N2) (''N'' represents negatively charged, ''P'' represents positively charged porphyrin) were prepared by reaction of the acid chloride of *meso*-monocarboxyphenylporphyrin and *meso*-*tetrakis*-carbo- xyphenylporphyrin, respectively, with tetramethylammonium(amino-*closo*-dodecaborate) (TMA-BNH_3) in DMF in the presence of pyridine. We studied the electrostatic association of these anionic boron containing porphyrins with different cationic porphyrin monomers (Fig. 1), 5-(3-methylpyridinum)-10,15,20-*tris*-phenylporphyrin iodide (P1), its zinc complex (P2), 5,10,15-*tris*-(4-tolyl)-20-(4-*N*,*N*,*N*-trimethylanilinium)porphyrin iodide (P3), and 5,10,15,20-*tetrakis*-(*N*-methylpyridinum-4-yl)porphyrin tetraiodide (P4), affording novel non-covalent dimeric and pentameric porphyrin arrays. *N*,*N*′-Dimethyl-4,4′- bipyridinium was also used to form a linker between two mono-anionic species (P1). The electrostatic interaction of a cationic quinone, namely 2(β-trimethyl-ammoniumethyl)benzoquinone bromide, with N1 or N2 yields porphyrin–quinone assemblies. The electrostatic association in solution was confirmed by UV–Vis, fluorescence and resonance light scattering (RLS) experiments [8], which showed an indication of the binding of the oppositely charged units under investigation.

The influence of anion–cation interactions on the structure and electronic absorption spectra of cationic porphyrins (P1–P4) and anionic porphyrins (N1) and (N2) was investigated. The spectral properties of these non-covalent linked porphyrins indicate the presence of electronic communication between the macrocycles in the ground and excited electronic state. The changes

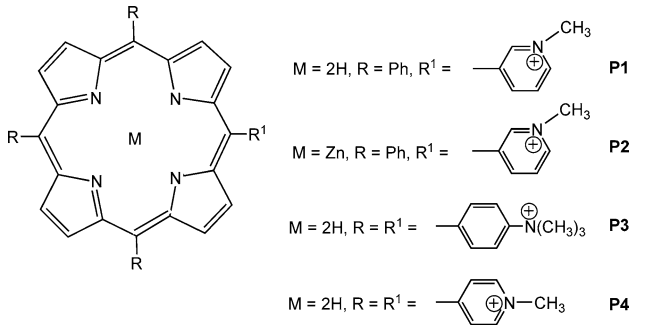

Fig. 1. Structure of cationic porphyrins P1–P4.

in absorption spectra of these assemblies can be attributed to the linear nature of the aggregated anionic porphyrin units. Therefore, the resulting oligomeric porphyrins are suggested as new donor–acceptor porphyrins which may be useful in electronic devices and as constant-potential electron reservoirs or electrically conducting ''molecular wires'' (which transmit energy and/or electron efficiently), if fashioned in linear configuration, [9]. These electrical properties of the assemblies are complementary to their photonic light-harvesting features.

2. Interactions of oppositely charged porphyrin units

Here, we report the prepartion of dimeric and pentameric non-covalent porphyrin assemblies. They are based on salt bridge formation between a negatively charged *closo*-dodecaborate-bearing porphyrin photodonor and positively charged porphyrin acceptor. Anionic porphyrins containing one and four polyhedral boron cages N1 and N2, respectively, were prepared as shown in Scheme 1. Mixing of concentrated aqueous or methanolic solutions of N1 or N2, respectivly and P1–P4 (Fig. 1), produces self-assembled dimeric or pentameric assemblies (Figs. 2 and 3) which can be isolated as solid products. In some assemblies such as P1 · N1, P3 · N1 and P4 · $(N1)_4$, the structure can be obtained from mass spectroscopy. The stoichiometry of the assembly (P:N) can be readily determined by several methods. In the application of Job's method [10] for the stoichiometry of cation–anion porphyrin aggregates studied, symmetrical curves were obtained which gave maxima at a mole fraction equal to 0.5 for the dimeric assemblies. Thus the stoichiometry was assumed to be 1:1. While the mole fraction was equal to 0.2 for the pentameric form. Further support has been observed in the ^{1}H NMR spectra which demonstrate 1:1 or 1:4 stoichiometric cation–anion porphyrin aggregates. Interstingly, both signals due to cationic and anionic moities can be observed independently. These simple spectroscopic characteristics directly give clear information on stoichiometry of present aggregation.

The ^{1}H NMR spectra of all the present assemblies show clear shift in the peripheral protons of the anionic units due to assembly formation. For example, the chemical shift of the B–H protons of boron cluster changed from the range 0.85–1.19 ppm to 1.16–1.42 ppm in its dimeric form P1 · N1. While a high field shift of 0.5 ppm was observed for the N–H protons in all the dimeric and pentameric forms. The inner N–H protons were slightly affected by aggregation in the pentameric assembly $(P2)_4$ · N2, where a high field shift of 0.2 was found. ^{1}B NMR spectra show that the B–N atom is affected by dimerization where the dimeric assemlies show downfield shift of 2.3 ppm.

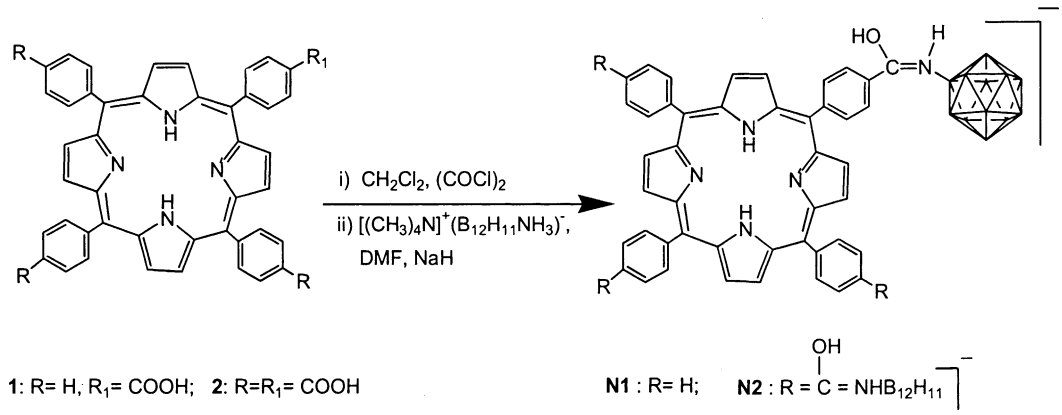

Scheme 1. Synthesis of anionic boronated porphyrins N1 and N2. In the cluster, each corner represents a boron atom, all but the N-substituted atom bearing an *exo*-H atom.

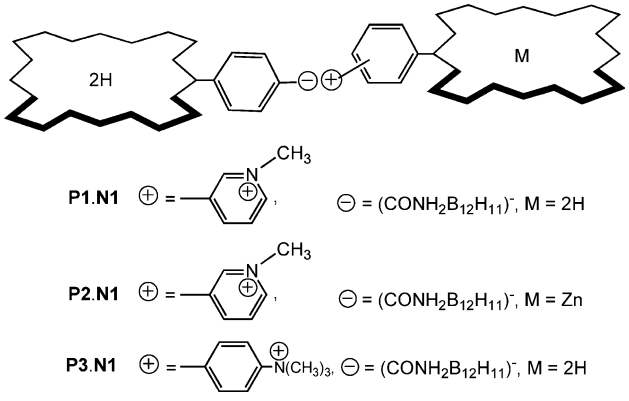

Fig. 2. Expected structure of dimeric porphyrin assemblies.

The vibrational frequencies of the B–H bond ν(B–H) and the B–B bond ν(B–B) were found to be slightly sensitive to aggregation. For N1 ν(B–H) is 2481 cm^{-1} and ν(B–H) varies from 2489 to 2496 cm^{-1} in the dimeric assemblies. Whereas, ν(B–H) for N2 is 2487 cm^{-1} and on pentamerization lies in the range 2466–2476 cm^{-1}.

These porphyrin or metalloporphyrin assemblies are soluble, to various degrees, in 5% DMSO/H_2O. The number (one or four) of the *meso* ionic groups on the axial unit determines whether the assemblies formed are dimeric or pentameric. Furthermore, the *meso*-monopyridyl porphyrin, and conceivably also the other porphyrin of the assembly, can be either free base or zinc-chelated, leading to a total of 16 different possible assemblies.

UV–Vis spectra of these assemblies were not merely the sum of its constituting monomer spectra. Figs. 4–7 show some examples of the absorption spectra of the monomeric ionic porphyrins and their mixture, all at the same molar concentration of each porphyrin. The characteristics of the absorption spectra of the porphyrin

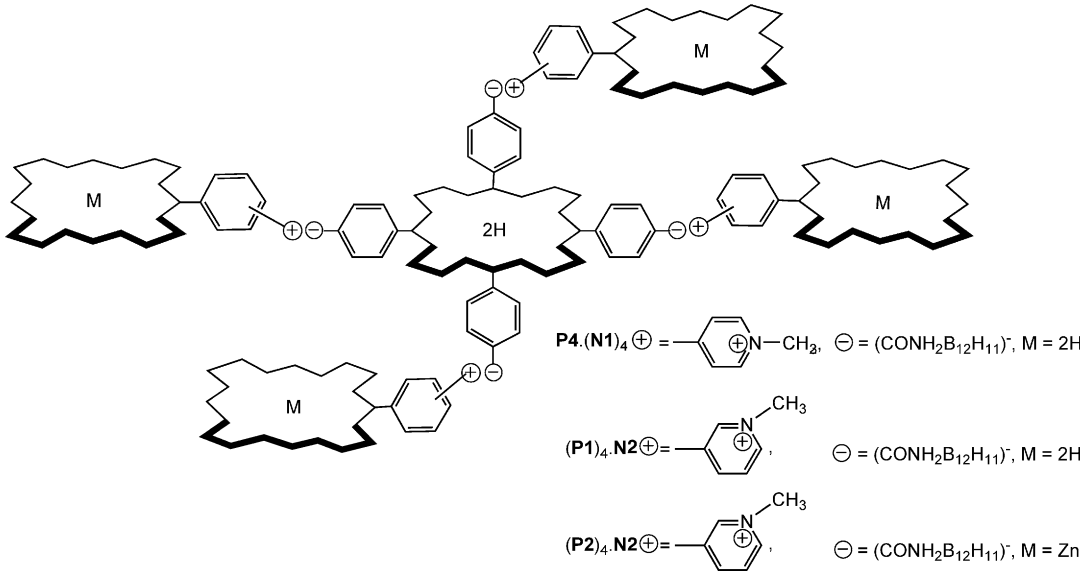

Fig. 3. Expected structure of pentameric porphyrin assemblies.

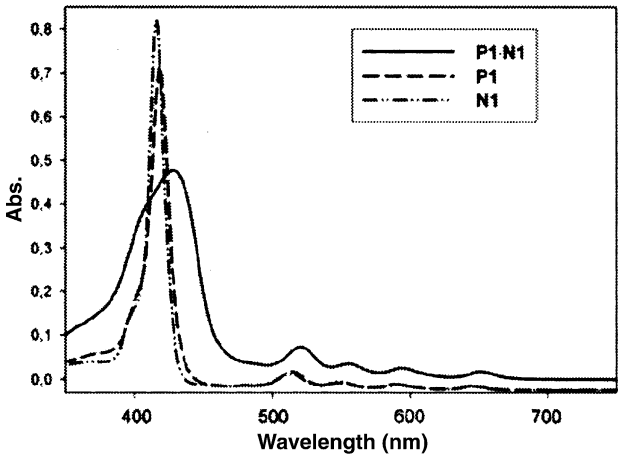

Fig. 4. Electronic absorption spectra of P1 · N1 dimer and its individual components in methanol at 2×10^{-5} M.

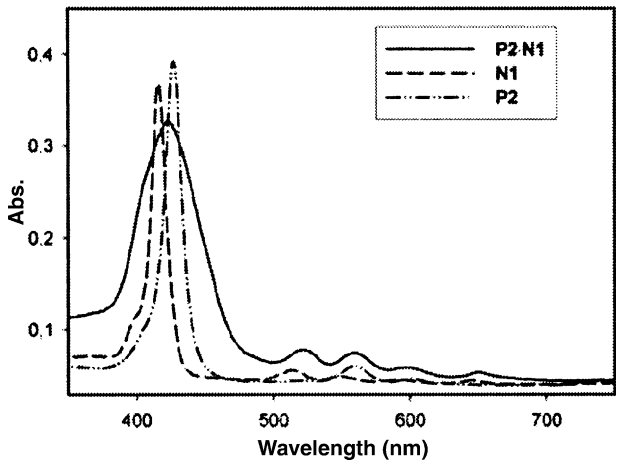

Fig. 5. Electronic absorption spectra of P1 · N1 dimer and its individual monomers in methanol at 10^{-5} M.

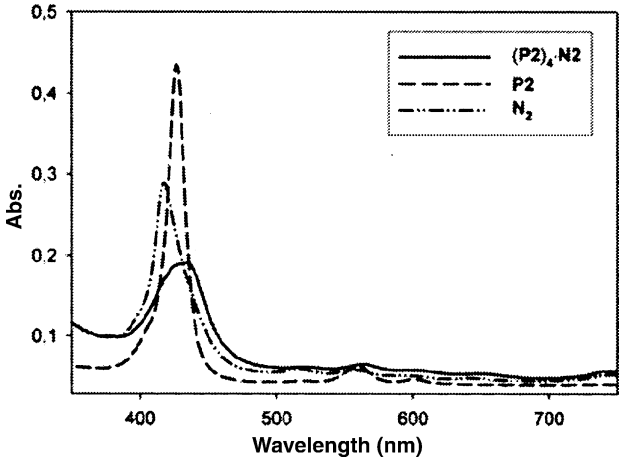

Fig. 6. Electronic absorption spectra of $(P2)_4 \cdot N2$ pentamer and its individual components in methanol at 10^{-5} M.

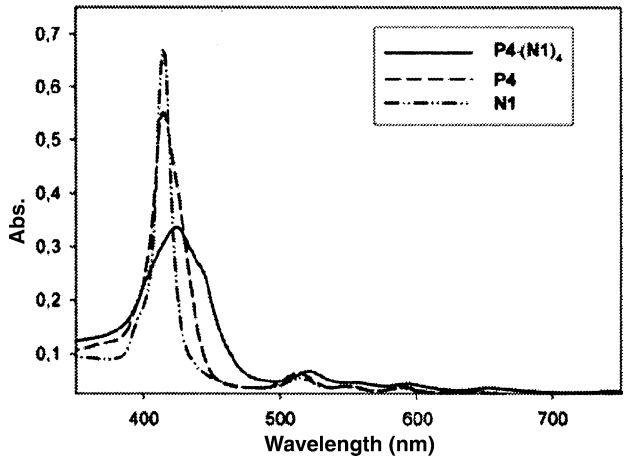

Fig. 7. Electronic absorption spectra of $P4 \cdot (N1)_4$ and its individual components in methanol at 2×10^{-5} M.

Table 1
Absorption spectra of non-covalent assemblies and their individual monomers, dissolved in methanol at 1×10^{-5} M[a]

Compound	λ_{max} ($\varepsilon \times 10^{-3}$, M^{-1} cm^{-1} (nm)
P1	417(576), 513, 549, 591, 647
P2	424(570), 560, 603
P3	417(539), 515, 549, 591, 647
P4	416(548), 514, 549, 591, 647
N1	416(560), 513, 549, 591, 647
N2	417(543), 515, 549, 592, 647
P1 · N1	421(245), 524, 558, 594, 653
P2 · N1	420(321), 521, 560, 592, 653
P3 · N1	420(251), 519, 556, 593, 650
$(P2)_4 \cdot N2$	429(212), 521, 560, 592, 656
$(P1)_4 \cdot N2$	419(247), 524, 558, 593, 653
$P4 \cdot (N1)_4$	423(234), 521, 557, 593, 653
N1 · bpy · N1	422(238), 522, 557, 594, 655

[a] In all cases, the solutions contained 0.1% DMSO used to dissolve the porphyrins.

assemblies are summarized in Table 1. The Soret band is much broadened and/or red shifted, showing a large hypochromicity in the Soret region of the dimer or pentamer. The decrease in the intensity of the Soret band, most sharply in the assembly $(P2)_4 \cdot N2$, indicates the electronic communication of the porphyrin units. The Q-bands are also broadened and slightly red shifted. Similar behavior of Soret bands are sometimes observed for the covalently linked porphyrin arrays and are illustrated by the theory of exciton coupling between chromophores [11]. The characteristic broadening of the Soret bands found for these systems strongly indicates that the porphyrin units are arranged in an array mode and approach each other within the range of exciton coupling interactions. The same behavior of the Soret band appears also, and to about the same extent, in the arrays containing zinc–porphyrin units P2 · N1 and $(P2)_4 \cdot N2$ as shown in Figs. 5 and 6, respectively. Taking into account exciton coupling and allowed transitions [12,13], the transitions with the highest dipole

moment, i.e., the Soret band in the case of porphyrins, are more affected. A red shift in the Soret band is predicted from head-to-tail association with in-line transition dipoles. These changes in absorption spectra of these assemblies can be attributed to the linear nature of the aggregated anionic porphyrin units. In order to check possible effects of the mutual orientation of the porphyrin rings, an analogous series of assemblies was synthesized with 3-*N*-methylpyridyl substituents (P1 and P2) as connecting groups. It showed the same changes as with the 4′-trimethylammoniumphenyl and 4′-pyridyl groups P3 and P4, respectively, as a connecting group, also reflecting the linear geometry of the resulting assembly.

The photophysical behavior of the resulting systems showed that both the anionic units are perturbed, as indicated by total fluorescence quenching of all assemblies with the exception of P2 · N1 and P4 · N1, where the fluorescence is partially quenched but not shifted.

3. Aggregation of P1–4 and N1–2 in aqueous solution

In methanolic or aqueous solution P4 obeys the Beer–Lambert law over a wide range of concentrations, therefore appears to remain in monomeric form in methanolic or aqueous solution. While P1 tends to form aggregates only in aqueous solution as shown in Fig. 8, its absorption spectrum shows the appearance of an intense new Soret band at 445 nm with a red shift in the Q-bands. The zinc complex P2 does not aggregate in contrast to the free base form neither in methanolic nor in aqueous solution as judged by UV–Vis. The UV–Vis spectrum of P3 in aqueous solution indicates the presence of aggregated forms due to the considerable broadening and hypochromaticity in the Soret band (not shown). The negatively charged boronated porphyrin N1 also has some aggregation and this is obvious from its absorption spectrum in water

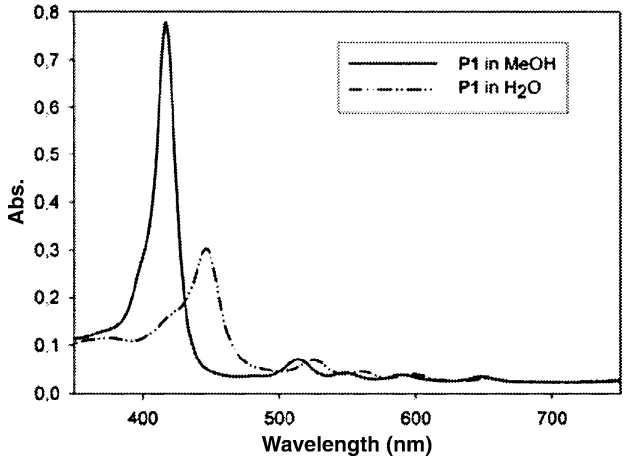

Fig. 8. Electronic absorption spectra of P1 in methanol and in 20 mM phosphate buffer, pH 7.1 at 2×10^{-5} M.

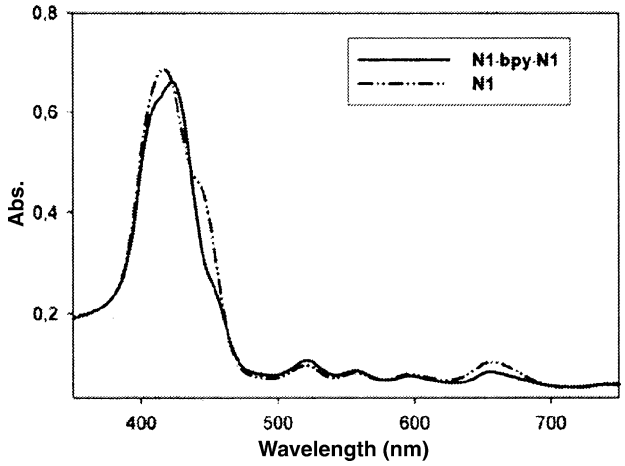

Fig. 9. Electronic absorption spectra of bipyridine linked dimer and its monomeric form in phosphate buffer, pH 7.1 at 2×10^{-5} M.

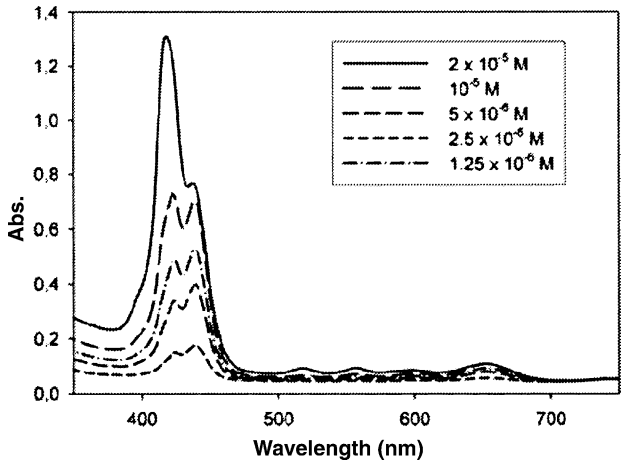

Fig. 10. Electronic absorption spectra of N2 at different concentrations in phosphate buffer, pH 7.1.

shown in Fig. 9 compared to methanol (Fig. 4). N2 tends to form aggregates in aqueous solution especially at lower concentrations (Fig. 10). There is an equilibrium between the monomeric and the aggregated form at 5 μM, and below this value the aggregated form represents the majority. The aggregation behavior of these ionic porphyrins indicates the formation of *J*-aggregates [14] in which the dipole moments of the monomers interacting in *J*-aggregates are parallel to the line connecting their centers, and are characterized by a red shift of the Soret band. While *H*-aggregates (blue shift in Soret band) break up rapidly upon dilution, *J*-aggregates are known to dissociate to monomers very slowly in aqueous solution.

4. RLS in the Soret absorption band

Recently, Pasternack et al. [8] found that aggregates of charged porphyrins in solution and on DNA template exhibit very strong light scattering at wavelengths,

450–490 nm, where only large aggregates have strong Soret absorption bands. Hence, a plot of the intensity of scattered light versus wavelength resembles the absorption spectrum of porphyrin aggregate. RLS cannot detect the dimers or pentamers expected from the present porphyrines, but it is suitable for detection of higher aggregates.

Although absorption spectra do not show the presence of aggregation in the case of P2 and P4, RLS experiments as a more sensitive method for detecting aggregation showed that all the studied ionic porphyrins do aggregate to different degrees in solution. The intensity of the RLS peak depends on the size of the aggregated form. In general the aggregation of those ionic porphyrins in aqueous solutions is higher than in methanol. RLS also proved the formation of *J*-aggregates in N2, where the intensity of RLS peaks of the aggregated monomers increases on dilution. If the association of oppositely charged porphyrins perturbed the aggregation of each monomer, and consequently led to a decrease in the intensity of RLS, then this could be considered as an indication of the combination of ionic porphyrin units in solution.

P1 has a tendency of forming porphyrin aggregates in aqueous solution giving enhanced light scattering at 446 nm, while N1 shows a low intensity RLS peak at 468 nm. Mixing of equal molar concentrations of N1 and P1 resulted in a decrease in the intensity of the RLS peak (Fig. 11) of P1, which can be attributed to the formation of oppositely charged porphyrin dimers and break-up of aggregates of the pure form.

P2 · N1, P3 · N1, P4 · $(N1)_4$, $(P1)_4$ · N2, and $(P2)_4$ · N2 follow the same behavior, where on mixing the RLS intensity of each monomer decreases sharply. Variation of pH has no effect on the interaction of oppositely charged porphyrin units except a slight decrease in RLS peaks of the mixed solutions on going from pH 0–7.

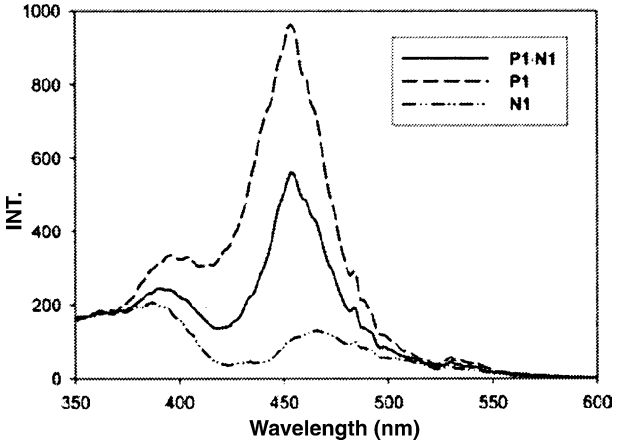

Fig. 11. RLS of P1 · N1 and its individual components in phosphate buffer, pH 7.1 at 10^{-5} M.

5. Interaction of N1 with bipyridine dication

As mentioned before, N1 aggregates in aqueous solution, reflected in its absorption and RLS spectra. When *N*,*N*′-dimethyl-4,4′-bipyridinium (bpy) was used in a ratio 1:2 as a spacer between two negatively charged porphyrin units, the resulting dimer has a red shifted Soret band (5 nm) compared to the monomer, with nearly complete disappearance of the peak assigned to aggregates (Fig. 9), reflected in a decrease in the RLS peak detected (not shown). This change in absorption spectrum was accompanied by total quenching of the fluorescence. These results seem to be in accord with assembly formation of N1 with the dication unit forming a linear bipyridine linked dimer.

6. Interaction of negatively charged porphyrins with cationic quinone

The first porphyrin–quinone systems which were developed in the 1970s, were molecules consisting of synthytic porphyrins covalently linked to quinones. The first excited singlet state of the porphyrin is a strong reductant and is easily observed by flash kinetics. Following absorption of light, the porphyrin transfers an electron to the quinone resulting a charge-separated state constiting of a cationic radical $P^{\cdot+}$ and an anionic $Q^{\cdot-}$. The interaction between negatively charged porphyrin and positively charged quinones is an easy method to obtain important: donor–acceptor systems. 2(β-Trimethyl-ammoniumethyl)benzoquinone bromide was chosen in this study. UV–Vis spectra indicate the presence of electronic interaction between the oppositely charged units, reflected in the red shift (7 nm) of the Soret band with a decrease in aggregation of the monomeric porphyrin, as depicted from its absorption spectrum in aqueous solution. Interaction of N1 with quinone partially quenches the fluorescence of N1 with a blue shift of the emission from 650 to 645 nm. RLS supports this result where the RLS peak of the porphyrin decreases on mixing (not shown). Interaction of N2 with quinone leads to blocking the negative charges in porphyrin and this makes the porphyrin unable to aggregate in solution as shown in absorption spectrum, where the Soret peak of the aggregated form disappeared and the Soret band is blue shifted (Fig. 12). This interaction also leads to complete quenching of the fluorescence of N2 at all concentrations. RLS of N2 shows a weak RLS peak at 465 nm; the low intensity of this peak can be attributed to the small aggregate size. Mixing of quinone and porphyrin leads to the formation of a porphyrin–quinone assembly decreasing the aggregation of monomeric porphyrin and shifting the RLS peak from 468 to 452 nm (not shown). Both the changes in

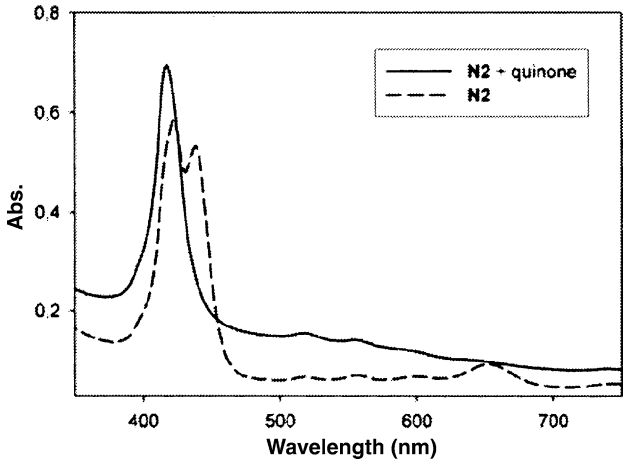

Fig. 12. Electronic absorption spectra N2-quinone assembly in phosphate buffer, pH 7.1 at 10^{-5} M.

absorption and RLS spectra confirm the interaction of N2 with quinone units.

7. Conclusion

In conclusion, the study presented here demonstrate that electrostatic interaction through salt bridges provides an easy route to generate (free base)porphyrin-(metallo)porphyrin assemblies avoiding the complexity represented in both linker formation and more importantly, selective metal insertion in the porphyrin subunits. Thus these systems are well adapted, through their ease of preparation, to study phenomena in mixed metalloporphyrin units. These results are a first step in the controlled formation of organized multimeric and polymeric porphyrin arrays of supramolecular nature. This methodology can be used to generate photoactive aggregates and to provide an effective pathway for mediating donor-to-acceptor electron and/or energy transfer. With respect to the previously investigated pentameric arrays that contain Zn and free base porphyrins, the systems reported here are expected to have excited states of the peripheral units higher than those of the central unit. In this case, however, the presence of the metal is likely to promote and govern very efficient intersystem crossing in the assembly which makes these systems suitable for the study of intercomponent energy transfer at the triplet, rather than at the singlet level. We hope that such systems can shed light on new aspects of photochemistry and photophysics of porphyrin aggregates.

8. Experimental

8.1. General

The reagents and all dry solvents were used as presented directly without further purification. The other chemicals were purchased from Aldrich or Fluka. *N*,*N*′-dimethyl-4,4′-bipyridylium diodide and decahydro-*closo*-dodecaborate $\{[(CH_3)_4N^+[B_{12}H_{11}NH_3]^-\}$ were prepared as described in the literature [15,16]. The measurements for NMR (^{11}B, ^1H and ^{13}C) were carried out on a Bruker DPX 200 spectrometer. The chemical shifts δ are given in ppm relative to $\Xi = 100$ MHz for δ (^1H) (nominally $SiMe_4$), and $\Xi = 32.083 \pm 972$ MHz for δ (^{11}B) (nominally F_3BOEt_2) in DMSO-d_6 and $CDCl_3$. IR (cm^{-1}) spectra were determined as KBr disc on a Biorad FTS-7 spectrometer. Mass spectra were recorded on a Finnigan MAT 8200 spectrometer. Plate and column chromatography was conducted on silica gel 60 (Fluka). UV–Vis-spectra were recorded on Varian Gary 50 Bio-Spectrometer. Fluorescence spectra were measured on Perkin–Elmer LS-50B-Fluorescence Spectrometer. RLS measurements were performed as in Pasternack et al. [8]. Briefly, samples were held in 1-cm quartz cuvettes. The excitation and emission monochromators of the Spectrometer were scanned synchronously (0.0 nm interval between association and emission wavelength), with detection at 90° relative to excitation. Unpolarized light was used to excite the sample and only unpolarized emission was detected.

8.2. Synthesis of cationic porphyrin monomers

5-(*N*-Methylpyridinum-3-yl)-10,15,20-*tris*-phenylporphyrin iodide (P1), its zinc complex P2 and 5,10,15,20-*tetrakis*-(*N*-methylpyridinum-4-yl)porphyrin tetraiodide (P4) were prepared according to the literature [17,18]. 5, 10, 15-*tris*-(4′-tolyl)-20- (4′-*N*,*N*,*N*-trimethylanilinium)porphyrin iodide (P3) was prepared from the corresponding mono-aminoporphyrin as described in the literature [19].

8.2.1. Tetramethylammonium[5-(benzamidodecahydro-closo-dodecaborate)-10,15,20-tris-phenylporphyrin] (N1)

5-(4′-Carboxyphenyl)-10,15,20-*tris*-phenylporphyrin [20] (900 mg, 13.77 mmol) was dissolved in 10 ml of dry CH_2Cl_2 of freshly distilled oxalyl chloride (1 ml) was added and the reaction was stirred at room temperature for 1 h. After distilling off the excess oxalyl chloride, the solvent was removed and the resulting acid chloride was dissolved in 10 ml dry dimethylformamide (DMF). TMA-BNHs (500 mg, 2.26 mmol) was dissolved in 10 ml dry DMF and the solution was cooled in ice. NaH (277 mg, 4.15 mmol, 60% suspension in oil) was added and the mixture was stirred for 30 min. This mixture was added dropwise to the acid chloride solution. Dry pyridine (0.3 ml) was added and the mixture was stirred for 24 h. The solvent was removed under reduced pressure and the crude product was purified twice by silica-gel TLC plate (MeOH/CH_2Cl_2 20%, $R_f = 0.42$) giving 320 mg (27%). ^1H

NMR (DMSO-d_6): δ −2.92 (bs, 2H, NH), 1.16–1.42 (m, 11H, BH), 3.1 (s, 9H, CH_3), 6.56 (m, 1H, NH), 7.67 (m, 9H, H_{arom}), 8.08 (m, 10H, H_{arom}), 8.73 (d, 8H, β-pyrrole). ^{11}B NMR (DMSO-d_6) −15.81 (s, 11B, B–H), −6.86 (bs, IB, B–N). IR 3415.3 (s, *v*-NH), 2481.6 (vs, *v*-BH), 1640.5 (s, *v*CO), 1450.2 (s), 1435.5 (s), 965.5 (m), 709.5 (m). MS (ESI): *m/z* 866 (M, 55%), 797 (M^{-1}, 25%). UV–Vis (MeOH): λ_{max} (ε $M^{-1}\,cm^{-1}$) 416 (560×10^3), 513, 549, 591, 647 nm.

8.2.2. *Meso*-tetrakis-(benzamidodecahydro-closo-dodecaborate)porphyrin (N2)

N2 was prepared as described for N1, by reaction of 200 mg (138 mmol) of *meso*-tetrakis-(4′-carboxyphenyl)porphyrin [21] with TMA-BNHs (117 mg, 176 mmol) by the previous procedure. The crude product was purified by TLC silica-gel plate (MeOH, $R_f = 0.3$) to give 153 mg (46%). ^{1}H NMR (DMSO-d_6): δ −2.93 (bs, 2H, NH), 0.82–1.6 (m, 44H, BH), 3.14 (s, 36H, CH_3), 4.16 (s, 4H, OH), 5.72 (bs, 4H, NH), 7.41 (d, 8H, 2,6-phenyl), 8.22 (d, 8H, 3,5-phenyl), 8.83 (s, 8H, β-pyrrole). ^{13}C NMR (DMSO-d_6) 55.39 (CH_3N^+), 118.73, 127.72, 128.97, 131.35, 135.38, 135.74, 141.2, 142.92, 175.59. ^{H}B NMR (DMSO-d_6):5 −15.33 (s, 44B, B–H), −5.97 (bs, 4B, B–N). IR 3772.4, 3680.7, 3618.8 (s, *v*-NH), 2939.8 (s, *v*-CH), 2487.2 (vs, *v*-BH), 1661.6 (s, *v*CO), 1628.8 (m, s, *v*-C═C), 1484.5 (s), 1350.7 (m), 796.5 (w). MS (ESI): *m/z* 1343 (M^{-4} + H, 30%). UV–Vis (MeOH): λ_{max} (ε $M^{-1}\,cm^{-1}$) 417 (543×10^3), 515, 549, 592, 647 nm.

8.3. Synthesis of non-covalent porphyrin assemblies

8.3.1. General procedure

A solution of the positively charged porphyrin P (0.01 mmol) was added to a solution of negatively charged porphyrin N (0.01 mmol) in 10 ml methanol at room temperature. The resulting precipitate was filtered and washed several times with MeOH giving P · N dimer. Pentamer P · $(N)_4$ and (N1 · bpy · N1) were prepared by the same procedure in ratio 1:4 of the corresponding charged porphyrin units and 2:1 porphyrin *N*,*N*′-bipyridinum salt, respectively.

8.3.2. P1 · N1 Dimer (yield = 56%)

^{1}H NMR (DMSO-d_6): δ −2.97 (bs, 4H, NH), 0.85–1.19 (m, 11H, BH), 4.64 (s, 3H, CH_3), 5.74 (s, 1H, OH), 6.03 (bs, 1H, NH), 7.81 (s, 19H, H_{arom}), 8.19 (d, 8H, H_{arom}), 9.01 (s, 16H, β-pyrrole), 8.82 (bs, 1H, 5′-pyridine), 9.48 (dd, 2H, 4′,6′-pyridine), 10.05 (s, 1H, 2′-pyridine). ^{11}B NMR (DMSO-d_6): δ −16.22 (s, 11B, B–H), −4.57 (bs, IB, B–N). IR 3436.2, 3114.5 (m, *v*-NH), 2982.8 (m, *v*-CH), 2489.5 (s, *v*-BH), 1612 (m, *v*C═C), 1470 (s), 1218.1 (s), 1046 (m) 761 (m). MS (ESI): *m/z* 1428 (M, 15%), 630 (P1, 100%), 796 (N1, 35%).

8.3.3. P2 · N1 Dimer (yield = 42%)

^{1}H NMR (DMSO-d_6): δ −2.97 (bs, 2H, NH), 0.75–1.24 (m, 11H, BH), 4.63 (s, 3H, CH_3), 5.70 (s, 1H, OH), 6.03 (bs, 1H, NH), 7.85 (s, 19H, H_{arom}), 8.19 (d, 8H, H_{arom}), 9.23 (s, 16H, β-pyrrole), 3.70 (bs, 1H, 5′-pyridine), 9.29 (dd, 2H, 4′,6′-pyridine), 9.96 (s, 1H, 2′-pyridine). ^{11}B NMR (DMSO-d_6): δ −15.92 (s, 11B, B–H), −4.76 (bs, IB, B–N). IR 3450.5, 3230.5 (m, *v*-NH), 289:5.7 (m, *v*-CH), 2487.8 (s, *v*-BH), 1608 (m, *v*C═C), 1318.9 (s), 1085 (m) 767 (m). MS (ESI): *m/z* 693 (P2, 95%), 796 (N1, 22%).

8.3.4. P3 · N1 Dimer (yield = 43%)

^{1}H NMR (DMSO-d_6): δ −2.96 (bs, 4H, NH), 0.8–1.92 (m, 11H, BH), 2.63 (s, 3H, CH_3phenyl), 3.89 (s, 9H, CH_3N^+), 5.71 (s, 1H, OH), 6.01 (bs, 1H, NH), 7.57 (d, 8H, 2′,6′-phenyl), 7.81 (bs, 7H, 3′,5′-phenyl), 8.03 (d, 8H, 3′,5′-phenyl), 8.18 (m, 6H, 2′,6′-phenyl), 8.46 (q, 6H, 2′,4′,5′-phenyl), 8.81 (m, 16H, β-pyrrole). ^{11}B NMR (DMSO-d_6): δ −16.21 (s, 11B, B–H), −4.57 (bs, IB, B–N). ^{13}C NMR (DMSO-d_6):5 21.94, 49.48, 57.59 (CH_3), 118.13, 120.19, 121.11, 125.95, 127.88, 128.56, 132.15, 132.51, 135.02, 136.09, 138.29, 139.08, 142.03, 143.86, 147.89. IR 3428.19, 3251.2 (s, *v*-NH), 2922.1 (m, *v*-CH), 2496.5 (s, *v*-BH), 1605 (s, *v*C═C), 1470 (s), 1350.5 (w), 1102.1 (w), 1023 (m), 966 (m) 980 (s). MS (ESI): *m/z* 1512 (M + 1, 20%), 714 (P3, 30%), 796 (N1, 15%).

8.3.5. P4 · $(N1)_4$ Pentamer (yield = 66%)

^{1}H NMR (DMSO-d_6): δ −2.97 (s, 10H, NH), 0.81–1.88 (m, 44H, BH), 4.78 (d, 8H, CH_3–N^+), 5.73, 6.07 (bs, 8H, NH), 7.26 (m, 8H, pyridine), 7.71, 8.00, 8.12 (m, 84H, H_{arom}), 8.75 (m, 48H, β-pyrrole + H_{arom}), 9.2 (d, 12H, pyridine). ^{11}B NMR (DMSO-d_6) −15.66 (bs, 44B, B–H), −5.12 (bs, 4B, B–N). IR 3412.8 (s, *v*-NH), 2476.4 (s, *v*-BH), 1633.5 (s, *v*C═O), 1603.5 (s, *v*C═C), 1471.5 (s), 1243 (s), 1023.7 (s) 799 (s). MS (ESI): *m/z* 694 (P4 + 1, 22%), 1354 (N1, 20%).

8.3.6. $(P1)_4$ · N2 Pentamer (yield = 55%)

^{1}H NM:R (DMSO-d_6): δ −2.98 (s, 10H, NH), −0.07–1.32 (m, 44H, BH), 4.63 (s, 12H, CH_3–N^+), 6.6, 6.8 (s, 8H, NH_2), 7.82–8.18 (m, 76H, H_{arom}), 8.82 (m, 40H, β-pyrrole), 9.02, 9.36, 9.99 (bs, 16H, pyridine). ^{11}B NMR (DMSO-d_6) −15.36 (s, 44B, B–H), −5.30 (s, 4B, B–N). IR 3372.8 (s., *v*-NH), 2466.4 (s, *v*-BH), 1650.5 (s, *v*C═O), 1600.9 (s, *v*C═C), 1381.5 (s), 1265 (s), 799 (s). MS (ESI): *m/z* 630 (P1, 30%), 3244 [$(P1)_2$N2, 70%].

8.3.7. $(P2)_4$ · N2 Pentamer (yield = 61%)

^{1}H NMR (DMSO-d_6): δ −3.09 (s, 10H, NH), 0.32–1.98 (m, 44H, BH), 4.62 (s, 12H, CH_3–N^+), 5.73, 6.07 (bs, 8H, NH), 7.97–8.35 (m, 80H, H_{arom}), 9.03–9.45 (m, 40H, β-pyrrole). ^{11}B NMR (DMSO-d_6) −15.30 (s, 44B, B–H), −5.12 (bs, 4B, B–N). IR 3372.8 (s, *v*-NH),

2466.4 (s, *v*-BH), 1650.5 (s, *v*C═O), 1600.9 (s, *v*C═C), 1381.5 (s), 1265 (s), 799 (s). MS (ESI): *m*/*z* 693 (P2, 70%), 1354 (N2, 60%).

8.3.8. Bipyridine linked dimer (N1 · bpy · N1) (yield = 41%)

^{1}H NMR (DMSO-d_6): δ −2.96 (bs, 4H, NH), 0.55–1.18 (m, 22H, BH), 4.42 (s, 6H, CH_3), 5.59 (bs, 4H, NH,OH), 7.35–8.21 (m, 42H, H_{arom}), 8.81 (d, 16H, β-pyrrole), 9.24 (d, 4H, pyridine). ^{11}B NMR (DMSO-d_6) −15.84 (s, 22B, B–H), −6.42 (bs, 2B, B–N). IR 3413.6 (s, *v*-NH), 3040.6 (m, *v*-CH), 2489.6 (vs, *v*-BH), 1638.8 (m, *v*C═O), 1473 (s), 1437.8 (s), 1023.3 (s) 953.6 (m), 705.2 (m). MS (ESI): *m*/*z* 186 (bpy, 100%), 974 (M − N1, 10%).

8.4. 2(β-Trimethyl-ammoniumethyl)benzoquinone bromide

0.52 g (2.25 mmol) of 2,5-dimethoxyphenylethylamine [22] in 25 ml $CHCl_3$ was stirred at 40 °C with 10 ml of methyliodide for 3 h and then the solvent evaporated to dryness in vacuum. The residue was dissolved in 20 ml dry CH_2Cl_2 and 5 ml of BBr_3. The solution was stirred overnight and then the solvent was evaporated under vacuum. The resulting crude material was dissolved in acetonitrile and treated with silver oxide according to the literature [23] to yield 75% of the titled compound. ^{1}H NMR (DMSO-d_6): δ 2.77 (d, 2H, CH_2), 2.93 (d, 2H, CH_2), 3.79 (s, 9H, CH_3), 6.77 (s, 3H, H_{arom}). MS (FAB): *m*/*z* 194 (M^+, 12%), 79 (Br^-, 15%).

8.4.1. N1-quinone dyad

^{1}H NMR (DMSO-d_6): δ −2.98 (bs, 2H, NH), 0.89–1.22 (m, 11H, BH), 2.97 (d, 2H, CH_2), 2.63 (d, 2H, CH_2), 4.04 (bs, 9H, CH_3), 5.05 (t, 4H, CH_2), 6.47 (b, 1H, NH), 6.82 (s, 3H, H_{arom}), 7.07–8.22 (m, 19H, H_{arom}), 8.82 (d, 8H, β-pyrrole. ^{11}B NMR (DMSO-d_6) −15.71 (s, 11B, B–H), −6.53 (bs, IB, B–N). IR 3415.3 (s, *v*-NH), 2481.6 (vs, *v*-BH), 1640.5, 1710.3 (s, *v*CO), 1440.2 (s), 1434.5 (s), 965.5 (m), 709.5 (m). MS (ESI): *m*/*z* 843 (M^- + 2Na, 45%), 196 (M^+, 20%), 797 (M^-, 50%). UV–Vis (H_2O): λ_{max} (ε, $M^{-1}\,cm^{-1}$) 423 (370×10^3), 522, 551, 593, 652 nm.

References

[1] E.B. Fleischer, Inorg. Chem. 1 (1962) 493.
[2] M. Krishnamurthy, Indian J. Chem. 15 (1977) 964.
[3] R.J. Fiel, J.C. Howard, E.H. Mark, D.N. Gupta, Nucleic Acids Res. 6 (1979) 3039.
[4] A.K.S. Chauhan, A. Kumar, R.C. Srivastava, J. Beckmann, A. Duthio, R.J. Butcher, J. Organomet. Chem. 689 (2004) 345.
[5] W.H. Sun, T. Zhang, L. Wang, Y. Chen, R. Froehlich, J. Organomet. Chem. 689 (2004) 43.
[6] E. Ojadi, R. Selzer, H. Linschitz, Am. Chem. Soc. 107 (1985) 7783.
[7] N.N. Kruk, O.P. Parkhots, N.V. Ivashin, J. Appl. Spectrosc. 68 (2001) 924.
[8] R.F. Pasternack, P.J. Collings, Science 269 (1995) 935.
[9] P.W. Kenney, L.L. Miller, J. Am. Chem. Soc. 123 (2001) 5835.
[10] P. Job, Ann. Chim. 10 (1928) 113.
[11] A.S. Davidov, Theory of Molecular Excitons, Plenum Press, New York, 1971.
[12] M. Kasha, A.M. El-Bayoumi, H.R. Rawls, Pure Appl. Chem. 11 (1965) 371.
[13] J.M. Ribo, J.M. Bofill, J. Crusats, R. Rubires, Chem. Eur. J. 7 (2001) 2733.
[14] P. Kubat, K. Lang, P. Anzenbacher, K. Jursikova, V. Kral, B. Ehrenberg, J. Chem. Soc., Perkin Transl. (2000) 933.
[15] P. Mentha, J. Am. Chem. Soc. 77 (1955) 6393.
[16] W.R. Hertler, M.S. Raasch, J. Am. Chem. Soc. 86 (1964) 3661.
[17] G.N. Williams, R.F. Williams, D. Lewis, Inorg. Nucl. Chem. 41 (1979) 41.
[18] T. Kaufman, B. Shamsai, R.S. Lu, R. Bau, G.M. Miskelly, Inorg. Chem. 34 (1995) 5073.
[19] S.A. Syrbu, A.S. Semeikin, T.V. Syrbu, Chem. Heterocycl. Comp. 32 (1996) 573.
[20] C.E. Kibbey, M.E. Meyerhoff, Anal. Chem. 65 (1993) 2189.
[21] L. Lindsey, J. Org. Chem. 45 (1980) 5215.
[22] T.E. Young, W.T. Beidler, J. Am. Chem. Soc. 49 (1984) 4833.
[23] E. Daniel, C. Daniel, Chem. Res. Toxicol. 13 (2000) 976.